Journal of Magnetism and Magnetic Materials 544 (2022) 168680

Contents lists available at ScienceDirect

Journal of Magnetism and Magnetic Materials

journal homepage: www.elsevier.com/locate/jmmm

Magnetic anisotropy in permalloy antidot square lattice

T.Y. Wang [a,b], H.-S. Han [c,d], C. Su [a,b,e], Q. Li [a,f], M. Yang [a,g], Weilun Chao [c], Xixiang Zhang [h], C. Hwang [i], A. Zettl [a,b,e], M.Y. Im [c], Z.Q. Qiu [a,b,*]

[a] Department of Physics, University of California at Berkeley, Berkeley, CA 94720, USA
[b] Materials Sciences Division, Lawrence Berkeley National Laboratory, Berkeley, CA 94720, USA
[c] Center for X-ray Optics, Lawrence Berkeley National Laboratory, Berkeley, CA 94720, USA
[d] Department of Materials Science and Engineering, Ulsan National Institute of Science and Technology (UNIST), Ulsan 44919, Republic of Korea
[e] Kavli Energy NanoScience Institute at the University of California, Berkeley, CA, USA
[f] National Synchrotron Radiation Laboratory, University of Science and Technology of China, Hefei, Anhui 230029, China
[g] Institute of Physical Science and Information Technology, Anhui University, Hefei, Anhui 230601, China
[h] Physical Science and Engineering Division (PSE), King Abdullah University of Science and Technology (KAUST), Thuwal 23955-6900, Saudi Arabia
[i] Korea Research Institute of Standards and Science, Yuseong, Daejeon 305-340, Korea

A B S T R A C T

Magnetic anisotropy of Permalloy (Py) antidot square lattice was investigated by torquemetry method using Rotation Magneto-Optic Kerr Effect (ROTMOKE). We find that there exists a field-dependent 4-fold magnetic anisotropy with the easy magnetization axis along the [11] axis of the antidot square lattice. In addition, there also exists an artifact of a uniaxial magnetic anisotropy in ROTMOKE result. We show that both results are due to the period wiggling of the magnetization in space which was confirmed by magnetic imaging using magnetic transmission soft x-ray microscopy (MTXM). Micromagnetic simulation from MuMax3 supports the wiggling structure of the magnetization, as well as reproduces ROTMOKE result. A simplified model was developed based on the periodic wiggling of the magnetization and successfully explored the physical origin of the field-dependent 4-fold anisotropy and the artifact of the uniaxial anisotropy.

1. Introduction

Magnetic nanostructures have attracted much interest due to their novel magnetic properties as well as their application potentials in spintronics technology [1]. While layered magnetic nanostructures usually employ interfacial/interlayer interactions to generate various magnetoelectronic properties such as the giant magnetoresistance [2,3] and tunneling magnetoresistance [4,5], magnetic dots/antidots are generally aimed to modulate spins laterally to create new magnetic states such as spin ice states [6], and magnetic vortices/skyrmions [7–9]. For the latter topic of magnetic dot/antidot nanostructures, array of periodically distributed dots or holes (antidots) are usually created to modulate the magnetization of a thin film at sub-micron length scale using various methods such as lithography, shadow mask growth, and self-assembly, etc [10].

In terms of experimental techniques, magnetic measurement usually involves two types of techniques, one measuring the macroscopic magnetization such as the torquemetry [11], hysteresis loop comparison [12], and Ferromagnetic Resonance (FMR) [13], etc., and the other probing the spatial distribution of the magnetization such as magnetic force microscopy (MFM) [14], photoemission electron microscopy (PEEM) [15], and scanning electron microscopy with polarization analysis (SEMPA) [16], etc. Each technique has its strength but also weakness. For example, macroscopic measurement can usually retrieve the anisotropy value from experiment but cannot reveal the microscopic origin. MFM has a high spatial resolution but probes only the stray field produced by the magnetic charges thus usually has to combine with micromagnetic simulation to reconstruct the in-plane magnetization distribution. In contrast, PEEM and SEMPA can probe magnetic component directly in all directions but have to be operated in the absence of external magnetic field. As a practical approach, there is a need to employ several complimentary measurement techniques in order to gain comprehensive information of the magnetic nanostructures.

In terms of magnetic properties in magnetic dot/antidot structures, magnetic anisotropy has been one of the intensely investigated properties because of its important role in high-density magnetic information technology [17,18]. The overall goal of this research direction is to achieve a tunable magnetic anisotropy [19] by tailoring the geometry of the system such as the shape, size, and spatial distribution of the dot/antidot, etc [20–22]. Most of the studies have taken the advantage of magnetic shape anisotropy that magnetic charges at the dot/antidot

* Corresponding author.
E-mail address: qiu@berkeley.edu (Z.Q. Qiu).

https://doi.org/10.1016/j.jmmm.2021.168680
Received 29 July 2021; Received in revised form 14 October 2021; Accepted 17 October 2021
Available online 22 October 2021

boundaries introduce additional magnetic dipolar interaction. A representative system is the square lattice of magnetic dots/antidots synthesized from a magnetic thin film. It was found that a 4-fold anisotropy could be induced in such system with the hard magnetization axis along the directions connecting nearest neighboring dots/antidots [13,23–26]. Although MFM images and numeric micromagnetic simulations suggest non-uniform spin configurations in the patterned nanostructures [23,27–29], direct determination of the in-plane magnetization remains elusive which obscures the relation between the magnetic anisotropy and the real-space spin configuration. Although there has been an argument that a uniform magnetization should not lead to a magnetic anisotropy in a square antidot array [23], it is unclear if such argument would still be valid as the antidot size becomes comparable to the antidot separation distance. In addition, it is puzzling that the anisotropy magnitude decreases with increasing the applied magnetic field even though such dependence offers a new opportunity to tailor the magnetic anisotropy [30].

In this paper, we report a systematic study of the magnetic anisotropy in permalloy (Py) antidot square arrays. Using rotational magneto-optic Kerr effect (ROTMOKE), we show a clear field-dependent four-fold magnetic anisotropy as well as an artifact of uniaxial anisotropy, indicating a physical origin of a spatial variation of the magnetization. By imaging the magnetic structure using full field magnetic transmission soft X-ray microscopy (MTXM), we directly revealed the in-plane wiggling structure of the Py magnetization and its behavior at different external magnetic fields. This spatial variation of the magnetization explains both the field-dependent four-fold anisotropy and the artifact of the uniaxial anisotropy in the ROTMOKE measurement. We further performed micromagnetic simulation and the result agrees nicely with the experimental observations. Finally, we offered a simplified model to reveal the physical origin of the 4-fold anisotropy and the artifact of the uniaxial anisotropy.

2. Experiment

Square lattice of Py antidots was prepared by depositing Py on top of Quantifoil holey carbon grid at room temperature by an e-beam evaporator in an ultrahigh vacuum system with a base pressure of 5×10^{-10} Torr. Py was chosen because it has negligibly small magnetic anisotropy so that magnetic anisotropy in Py antidot square arrays comes entirely from the patterned structure. The holey carbon grid is made of a 15 nm thick holey carbon film containing a square array of 1μ m-diameter circular holes with a center-to-center distance of 1.6μ m. Py film deposited on top of this holey carbon grid naturally forms a film with arrays of antidot forming at the locations of the holes. The circular shape of the antidot ensures that each dot alone does not generate magnetic anisotropy so that the macroscopic anisotropy has to come from the global antidot square lattice. SEM image confirms the formation of the Py antidot flat film with desired sizes (Fig. 1).

ROTMOKE measurement was performed at room temperature on the Py antidot sample. The in-plane projection of the incident laser beam was set to be parallel to the nearest neighbor antidots axis. As an in-plane magnetic field rotates in the film plane, the ROTMOKE measures the projection of the magnetization along the optical plane from which the angle between the magnetization and the optical plane could be retrieved. Then the angular difference between the magnetic field and the magnetization contains information of the magnetic anisotropy. Detailed description of the ROTMOKE instrument and principle can be found in our previous paper [31].

MTXM measurement was performed at room temperature at beamline 6.1.2 of the Advanced Light Source at Lawrence Berkeley National Laboratory. Off-orbit emitted radiation provides elliptically polarized x-rays which illuminates the sample after passing a condenser zone plate. Another micro zone plate then projects a full field image onto a CCD camera that is sensitive to soft x-rays. External magnetic field generated by a solenoid was applied along the sample surface. At the Fe L3 absorption edge (708 eV), the absorption of x-ray transmitted through the Py film depends on the relative angle between the beam direction and the local magnetization [known as x-ray magnetic circular dichroism (XMCD)], which gives magnetic contrast in the image [32]. To obtain the in-plane magnetic components, the sample was mounted at 60° angles with respect to the x-ray propagation direction.

As shown in the next section, a combination of ROTMOKE, MTXM, and micromagnetic simulations offers a comprehensive understanding of the fundamental origin of the antidot-induced magnetic anisotropy.

3. Result and discussion

3.1. MOKE and ROTMOKE result

We first present the result of hysteresis loop measured by magnetic-optic Kerr effect (MOKE) and torque curve measured by ROTMOKE on a 70 nm thick Py antidot array. [10] and [11] directions of the antidot square array are defined in Fig. 1. Hysteresis loops for magnetic field along [10] and [11] axes in Fig. 2 show clearly that it is easier to saturate the magnetization in [11] direction than [10] direction, showing that the magnetic easy axis is parallel to [11] axis.

Next, we present the ROTMOKE result. For an in-plane magnetic field applied to the film with uniform magnetization, the magnetic energy per unit volume is

$$E = -HM_S\cos(\theta-\varphi) - K_2\cos^2(\varphi-\varphi_2) + K_4\sin^2(\varphi)\cos^2(\varphi) \quad (1)$$

where M_S is the saturation magnetization, H is the magnitude of the

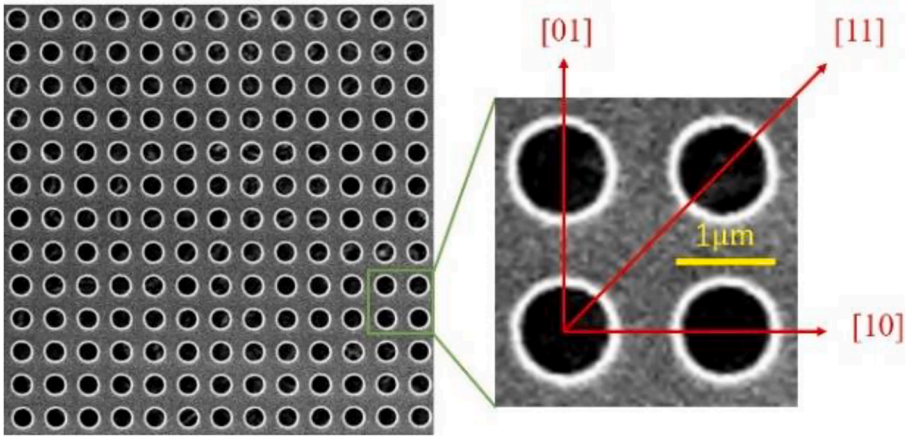

Fig. 1. SEM image of 70 nm-thick Py antidots square array on Quantifoil holey carbon grid.

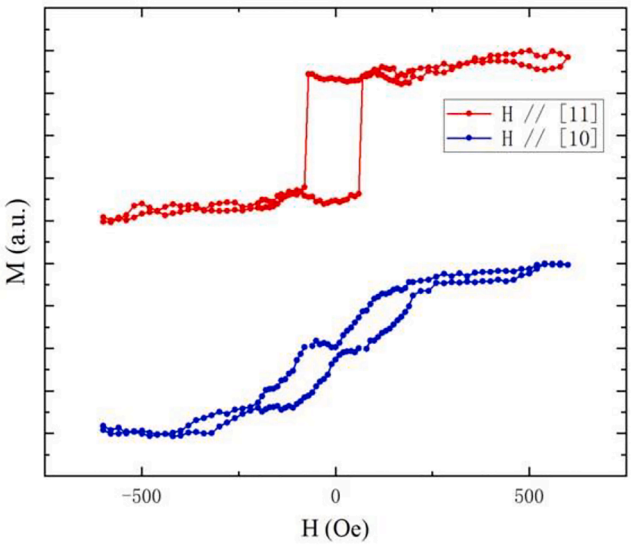

Fig. 2. Hysteresis loop along [10] and [11] directions of the Py antidot square lattice measured by MOKE. Hysteresis loop fully closes at around 500 Oe.

applied magnetic field, K_2 is the uniaxial magnetic anisotropy, K_4 is the 4-fold magnetic anisotropy, and θ and φ are the angles of the magnetic field and the magnetization relative to the [10] direction of the antidots lattice, respectively. φ_2 defines the easy ($K_2 > 0$) or hard ($K_2 < 0$) magnetization axis of the uniaxial magnetic anisotropy. Minimizing the energy with respect to φ leads to the magnetic torque [$l(\varphi)$] needed to achieve equilibrium state.

$$l(\varphi) \equiv Hsin(\theta - \varphi) = \frac{1}{2}H_{K_2} sin[2(\varphi - \varphi_2)] + \frac{1}{4}H_{K_4}\sin(4\varphi) \quad (2)$$

where $H_{K_2} = 2K_2/M_s$, $H_{K_4} = 2K_4/M_s$ are the uniaxial anisotropy and 4-fold magnetic anisotropy fields, respectively.

To have a unique magnetic torque at a given magnetic field, the field has to be strong enough to wipe out all irreversible magnetic domains. Therefore, we performed ROTMOKE measurement with the magnetic field greater than ~500 Oe above which the hysteresis disappears even along the hard axis (Fig. 2). It should be noted that the magnetizations of Py antidots film are not saturated to have all spins in exact the same direction during the ROTMOKE measurement, as will be shown in MTXM images later in this paper. For a given direction of the field (θ), the magnetization angle (φ) is determined from the ROTMOKE signal which is proportional to cosφ. Then the magnetic torque of $Hsin(\theta - \varphi)$ is constructed as a function of φ. Fig. 3 depicts a representative ROTMOKE result at H = 600 Oe.

The magnetic torque oscillates with φ with a periodicity of 90° [Fig. 3(a)], showing the existence of a 4-fold magnetic anisotropy. Looking in details, the 4-fold oscillation of the torque does not have the same peak heights. In fact, the 1st and 3rd peaks have the same height which is less than the height of the 2nd and 4th peaks. This behavior indicates the existence of a uniaxial anisotropy ($H_{K_2} \neq 0$) in addition to the 4-fold anisotropy (H_{K_4}). A fitting of the experimental data using Eq. (2) yields $H_{K_2} = -104 \pm 4$ Oe, $\varphi_2 = -2.2 \pm 1.3^{\circ}$, and $H_{K_4} = -181 \pm 10$Oe. The negative value of H_{K_4} indicates that [10] and [01] axes are the hard magnetization axes and [11] and [1$\bar{1}$] axes are the easy magnetization axes of the 4-fold magnetic anisotropy.

In a system with a perfect 4-fold symmetry, uniaxial magnetic anisotropy is forbidden. However, uniaxial anisotropy could be induced by breaking the 4-fold symmetry such as by different lengths of the antidot along [10] and [01] axes [30] or by off-normal growth of the magnetic film [33]. We checked our sample carefully and find no evidence of elliptical shape of the antidots (Fig. 1). We also grew the Py carefully with normal directional growth by facing the evaporator

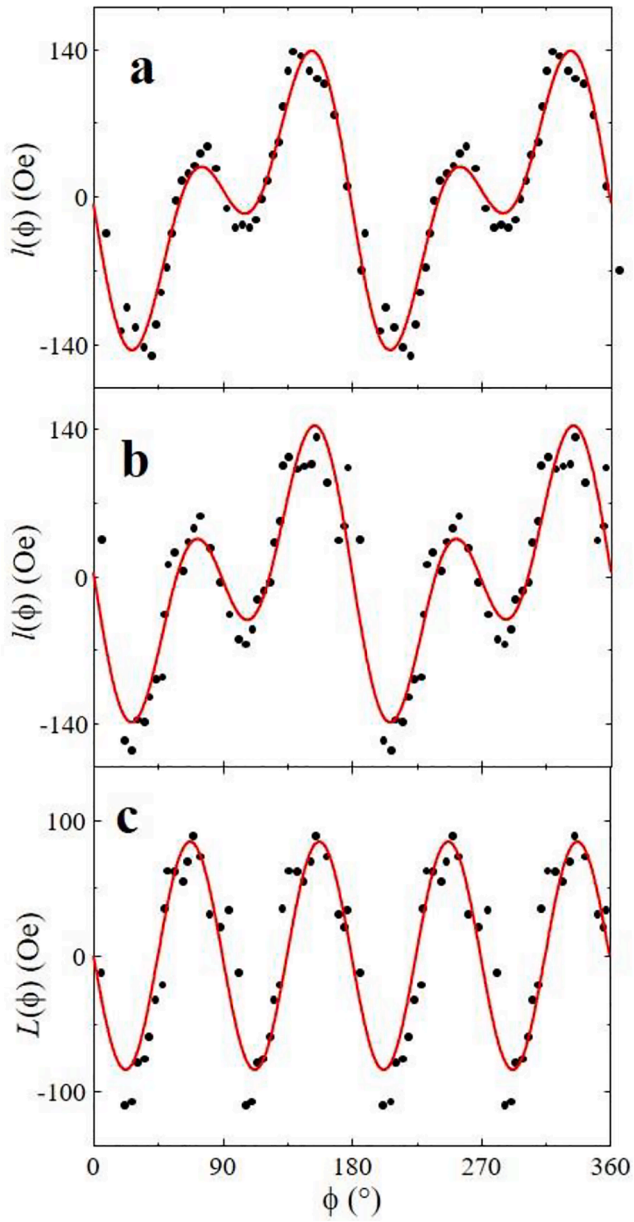

Fig. 3. ROTMOKE result. Magnetic torque $l(\varphi)$ at H = 600 Oe with the optical plane parallel to a, [10] axis, and b, [01] axis of the sample, respectively. In experiment, a and b were achieved by fixing the optical plane in space but rotating sample by 90° around the surface normal direction. The identical result of a and b shows that the uniaxial anisotropy is an artifact. c, Redefined torque $L(\varphi)$ using Eq. (3) to eliminate the artifact of the uniaxial anisotropy. Red lines are fitting curves using Eq. (2).

directly to the substrate. Therefore, we believe that the uniaxial anisotropy should be an artifact appeared in the ROTMOKE measurement. To prove this, we rotated the sample by 90° and performed the ROTMOKE measurement again. If the uniaxial anisotropy were a real existence in the sample, the easy magnetization axis of the uniaxial anisotropy would have been changed by 90° (e.g., φ_2 should increase by 90°) while keeping the 4-fold anisotropy unchanged. Consequently, the magnitudes of the four peaks in Fig. 3(a) would have been changed accordingly with the height of the 1st and 3rd peaks greater than the height of the 2nd and 4th peaks. Our ROTMOKE result after the sample rotation [Fig. 3(b)], however, is identical to the ROTMOKE result before the sample rotation [Fig. 3(a)]. In fact, the same fitting applied to Fig. 3 (a) fits Fig. 3(b) perfectly (red color solid line), proving that the uniaxial

anisotropy is an artifact in the ROTMOKE measurement rather than a real existence in the sample. We will discuss the origin of this artifact later in the paper.

To eliminate the artifact of the uniaxial anisotropy in the torque, we reinforce the 4-fold symmetry by redefining the torque as:

$$L(\varphi) = \frac{1}{2}\left[l(\varphi) + l\left(\varphi + 90^0\right)\right] \quad (3)$$

$L(\varphi)$ obtained in this way [Fig. 3(c)] eliminates the artifact of the uniaxial anisotropy and can be fitted using Eq. (2) with $H_{K_2} = 0$ to obtain the 4-fold anisotropy H_{K_4}. In fact, the H_{K_4} obtained in this way has the same value as the fitting result of H_{K_4} obtained from Fig. 3(a) within the error bar from the fittings.

Fig. 4 shows the fitting result of H_{K_4} (blue squares) above 500 Oe (below 500 Oe irreversible hysteresis appears so that ROTMOKE method is no longer valid). The result shows that the magnitude of the 4-fold anisotropy ($|H_{K_4}| = -H_{K_4}$) decreases with increasing the field, in agreement with result reported in literature [23]. Moreover, we find that the magnitude of the 4-fold anisotropy decreases monotonically with increasing the magnetic field. This behavior implies that the 4-fold magnetic anisotropy should vanish in the limit of $H \to \infty$. Note that magnetization becomes uniform ($\nabla \vec{M} = 0$) in the limit of $H \to \infty$ and that the magnetic charge distribution at the boundary of a circular disk with a uniform magnetization corresponds to a magnetic moment at the center of each antidot, the vanish of the 4-fold magnetic anisotropy is the expected fact that magnetic dipolar interaction should not give a 4-fold shape anisotropy for a uniform magnetization in a square lattice (we will give a rigorous proof of this assertion later in this paper). Therefore, the non-zero 4-fold magnetic anisotropy in our antidot square lattice must come from a non-uniform magnetization in space at finite magnetic field.

3.2. Magnetic images

To prove the inhomogeneity of the magnetization in space, we obtained magnetic images of 100 nm thick Py antidot square lattice using MTXM at room temperature. The MTXM images (Fig. 5) with an in-plane magnetic field show clearly that the magnetization is not aligned uniformly to the field direction. Instead, the magnetization tends to deviate away from the field direction especially at low magnetic field. In particular, the magnetization in region between two nearest neighbor antidots tends to be parallel to the antidot boundary, leading to a periodic wiggling of the magnetization around the antidot square lattice. The wiggling amplitude of the magnetic texture reduces gradually with increasing magnetic field, approaching a uniform saturation magnetization to the field direction as the in-plane field increases to 1 kOe which is the maximum in-plane field available at the MTXM beamline.

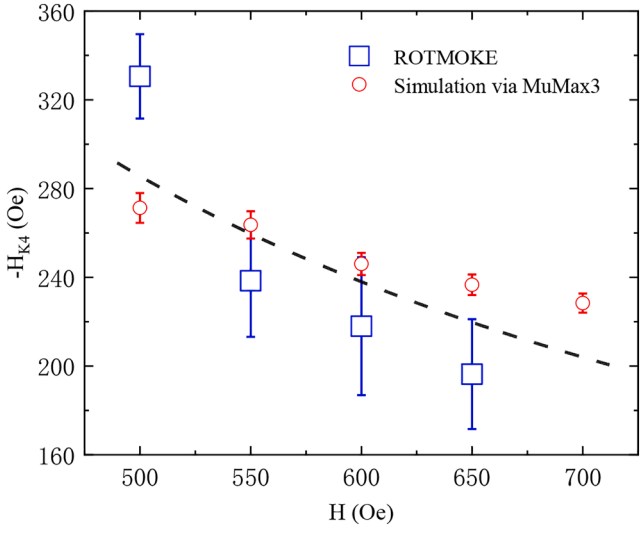

Fig. 4. Magnitude of H_{K4} from ROTMOKE experiment and MuMax3 simulation above 500 Oe. Dashed line represents $H_{K4} \propto 1/H$ relation from the simplified model.

Qualitatively, the wiggling of the magnetization can be understood by considering the magnetic charges at the antidot boundary. For a uniform magnetization along the field direction, magnetic charges are induced at the antidot boundary. To reduce the magnetic dipolar interaction energy, magnetic charges at the antidot boundary should be reduced by rotating the magnetization between two nearest neighbor antidots along [10] axis towards the [01] or [0$\bar{1}$] direction. Similarly, the magnetization between two nearest neighbor antidots along [01] axis should rotate towards [10] or [$\bar{1}$0] direction to reduce the magnetic charges at the antidot boundary. Therefore, a uniform magnetization in the field direction should rotate in opposite directions along the [10] and [01] axes to reduce the magnetic charges at the antidot boundaries, leading to a periodic wiggling of the magnetization in the antidot square lattice. Since this wiggling of magnetization is at the expense of Zeeman energy by rotating the magnetization away from the magnetic field direction, the wiggling amplitude should be obviously reduced by increasing the magnetic field.

3.3. Micromagnetic simulation

To have a quantitative analysis, we have to consider a continuous variation of the magnetization in whole space. To do so, we performed micromagnetic simulation using MuMax3 on a 100 nm Py thick antidot film with the same geometry parameters as in the experiment. The simulation result (Fig. 5) indeed shows the same trend of wiggling magnetization as observed by the MTXM with the wiggling amplitude decreasing with increasing magnetic field. Furthermore, we find that the wiggling magnetization follows exactly 4-fold symmetry as the magnetic field direction rotates. This is expected because in simulation we could ensure a prefect 4-fold symmetry of the antidot system.

Then the interesting question is whether an artifact of uniaxial anisotropy would appear in the ROTMOKE measurement from a simulation on a perfect 4-fold antidot square lattice? To answer this question, we performed micromagnetic simulation of the process of ROTMOKE via MuMax3 on a 10×10 Py antidot square lattice (70 nm Py thickness, 1μm-diameter hole, and 1.6μm period) for a rotating in-plane magnetic field of H = 500–700 Oe. For each step of the magnetic field angle (θ), equilibrium state of the magnetization in the MuMax3 simulation was achieved by relaxing the equilibrium state of the magnetization of the previous step. Because of the perfect 4-fold symmetry of our system, it turns out that simulation was needed only for $0^\circ \le \theta \le 90^\circ$ and simulation result for $90^\circ \le \theta \le 360^\circ$ can be simply obtained by extending the result of $0^0 \le \theta \le 90^0$ to the corresponding angular range. In this way, we obtained the magnetic state in the whole range of field angle from 0° to 360° with 5° per step. Next, for each field angle θ, we calculated the averaged projection of the magnetization to the [10] axis ($M_x = \frac{1}{N}\sum_{i=1}^{N} cos\varphi_i$) which is what ROTMOKE measures directly in experiment. The maximum value of M_x among all field angles is set to be the saturation magnetization (M_s) and then the averaged magnetization angle $\varphi \equiv \arccos\left(\frac{M_x}{M_s}\right)$ and magnetic torque $l(\varphi) = Hsin(\theta - \varphi)$ were obtained from the simulation and compared to the experimental ROTMOKE result. One of the simulated torque curves is shown in Fig. 6.

The $l(\varphi) vs \varphi$ relation obtained from the simulation agrees nicely with the ROTMOKE experiment result. H_{K_4} values obtained by fitting the simulated $l(\varphi) vs \varphi$ at several field strengths are shown in Fig. 4 for comparison with the experimental result. We would like to point out a few essential features from the simulation. First, it is clear that the magnetic anisotropy arises from the inhomogeneity of the magnetization in space, i.e., it is the wiggling of the magnetization in space that

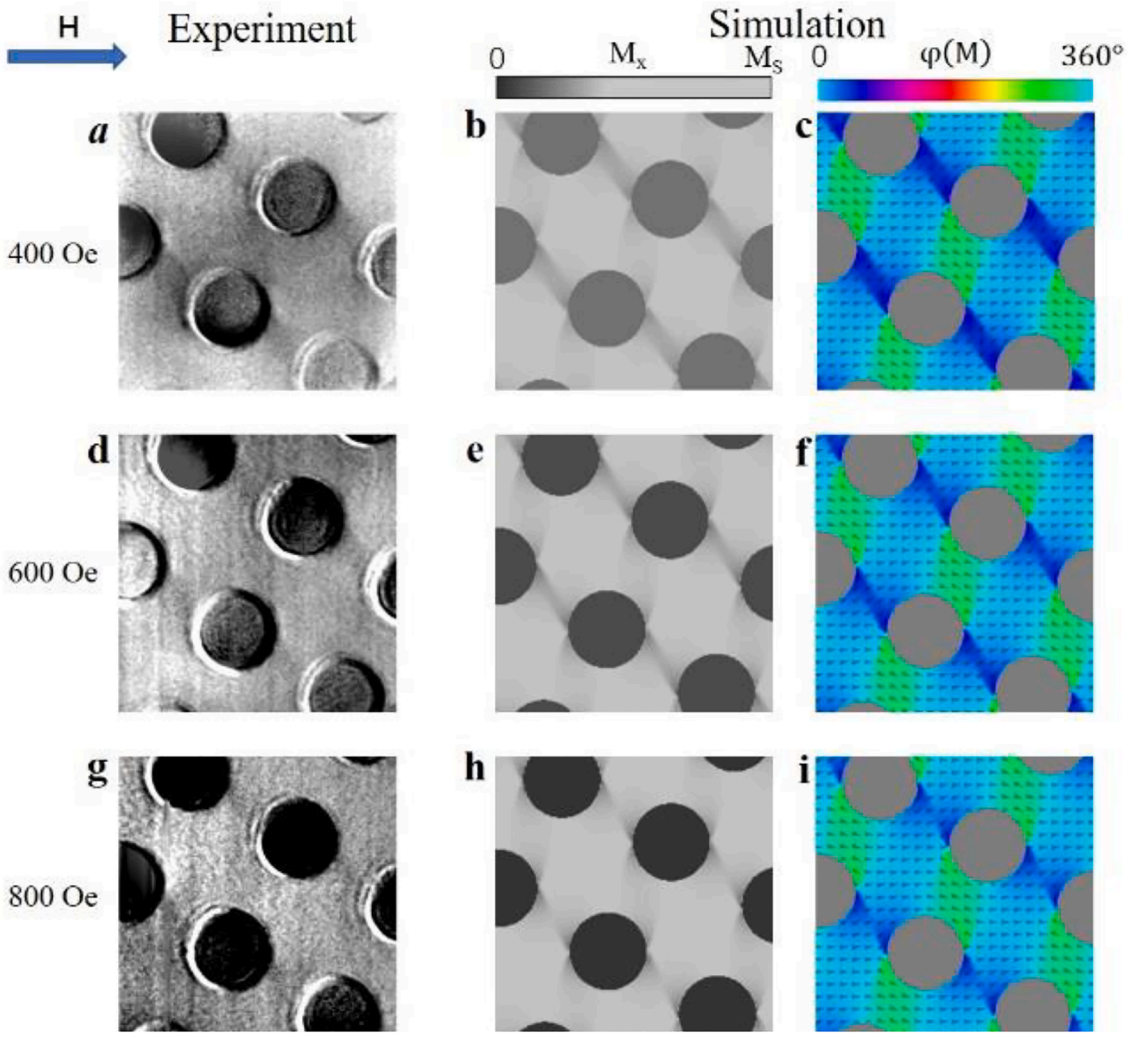

Fig. 5. Experimental images from MTXM and simulated images from MuMax3. a, d, g: Experimental MTXM images with in-plane magnetic field of 400, 600 and 800 Oe, respectively, along the magnetic field direction as shown on the top left. b, e, h: Simulated MTXM images with the x-component of magnetization (M_x) represented by the greyscale colormap shown on top. c, f, i: Colored images showing the magnetization direction in space. The colormap on top shows the magnetization angle φ(M) relative to the field direction.

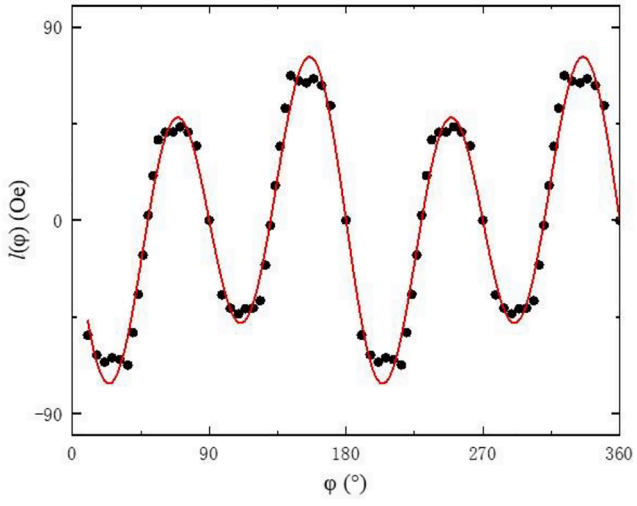

Fig. 6. An example of simulated torque $l(\varphi)$ via MuMax3 at H = 600 Oe.

makes the spatially averaged φ different from the θ. Specifically, it is the magnetization between nearest neighbor antidots, which prefers its orientation parallel to [10] or [01] axis, that results in the macroscopic magnetic anisotropy. Second, the different peak heights in $l(\varphi)$ (e.g., the 1st and 3rd peak heights are less than the 2nd and 4th peak heights) show that an artifact of uniaxial anisotropy appears in the simulated $l(\varphi)vs\varphi$ relation, in agreement with the experimental observation [Fig. 3 (a) and (b)]. As shown in the next section, it is the broadening of the angular distribution of the magnetization that leads to the artifact of the uniaxial anisotropy.

3.4. Simplified model

While the micromagnetic simulation successfully reproduces experimental result, physical origin of the result remains obscure in the numerical calculations except the fact that it is the spatial variation of the in-plane magnetization that is responsible for the magnetic anisotropy. To explore the physical origin, we here discuss a simplified model to explain the 4-fold magnetic anisotropy and the artifact of uniaxial anisotropy in terms of the magnetization wiggling in space. We start by considering a two-dimensional antidot square lattice in xy plane with an in-plane magnetization. The total dipolar energy of the system is

$$E_d = \sum \frac{\vec{m}(\vec{r})\cdot\vec{m}(\vec{r}') - 3\vec{m}(\vec{r})\cdot\left(\widehat{\vec{r}-\vec{r}'}\right)\vec{m}(\vec{r}')\cdot\left(\widehat{\vec{r}-\vec{r}'}\right)}{|\vec{r}-\vec{r}'|^3} \quad (4)$$

Using $\varphi(\vec{r})$ to specify the local angle between the local magnetic moment and the [10] axis of the antidot square lattice, it is easy to show that the change of the dipolar energy due to magnetization wiggling of $\varphi(\vec{r}) = \varphi_M + \delta\varphi(\vec{r})$ to the leading order of $\delta\varphi(\vec{r})$ is

$$\delta E_d = 3\sin(2\varphi_M)\sum \frac{[\delta\varphi(\vec{r}) + \delta\varphi(\vec{r}')][(x-x')^2 - (y-y')^2]}{2|\vec{r}-\vec{r}'|^5} \quad (5)$$

We have employed the result of $\sum \frac{\delta\varphi(\vec{r})(x-x')(y-y')}{|\vec{r}-\vec{r}'|^5} = \sum \frac{\delta\varphi(\vec{r}')(x-x')(y-y')}{|\vec{r}-\vec{r}'|^5} = 0$ in the derivation because of the inversion symmetry and the 4-fold symmetry of the antidot square lattice with circular shaped antidot.

For uniform magnetization, $\delta\varphi(\vec{r})$ is independent of position so that $\varphi(\vec{r}) = \varphi_M + const.$ corresponds to a uniform rotation of a uniform magnetization. Then Eq. (5) yields $\delta E_d = 0$ because a 4-fold symmetry yields $\sum \frac{(x-x')^2-(y-y')^2}{2|\vec{r}-\vec{r}'|^5} = 0$. This is the result mentioned in previous section that dipolar interaction from a uniform magnetization in a square antidot lattice with 4-fold symmetry does not give rise to any magnetic anisotropy.

To have a non-zero δE_d, the local magnetic moments at $\vec{r}$ and $\vec{r}'$, need to twist oppositely [e.g., $\delta\varphi(\vec{r})$) and $\delta\varphi(\vec{r}')$ have opposite signs] as $(x-x')^2-(y-y')^2$ changes its sign under the action of $x \leftrightarrow y$. This corresponds to the scenario that the magnetization between neighboring antidots along [10] axis rotates in opposite direction as the magnetization between neighboring antidots along [01] axis. In another word, the magnetization needs to wiggle oppositely along the [01] and [01] axes in order to give rise to a non-zero magnetic anisotropy of $\delta E_d \neq 0$, which is exactly what was observed in our experiment. The physical origin of the opposite twisting angles of the magnetization along [10] and [01] axes is that the region between nearest neighbor antidot holes along [10] axis prefer the magnetization along [01] axis due to local shape anisotropy, which is equivalent to a local uniaxial anisotropy with [01] axis being the magnetic easy axis. Similarly, the region between nearest neighbor antidot holes along [01] axis has an equivalent local uniaxial anisotropy with [10] axis being the magnetic easy axis. To make this physical picture clearer, we further simplify the model by breaking the magnetization texture into two subsystems of $\vec{M}_1$ and $\vec{M}_2$ with $\vec{M}_1$ and $\vec{M}_2$ experiencing local uniaxial anisotropies (K) of [10] and [01] easy magnetic axis, respectively, as shown in Fig. 7. Although not accurate, this simplified model can catch the physical origin of all experimental observations.

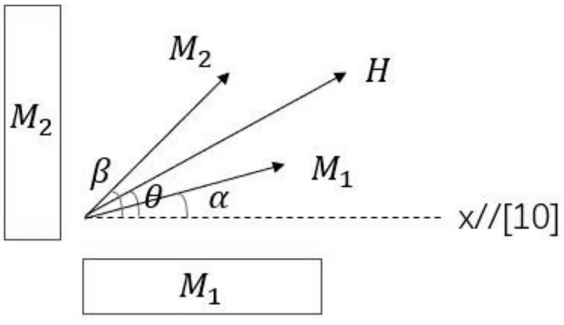

Fig. 7. Schematic drawing of the oversimplified model. M_1 and M_2 are the magnetizations of the two domains whose magnetic easy axes are parallel to [10] and [01] axes, respectively. As a magnetic field H is applied at an angle θ to the [10] axis, M_1 and M_2 will tilt away from the field direction towards their own easy axes, resulting in angles of α and β to the [10] axis. In the case depicted here, $\alpha < \theta < \beta$.

Without the two local uniaxial magnetic anisotropies or in the limit of $H \to \infty$, it is obvious that a uniform magnetization of $\vec{M}_1 = \vec{M}_2$ should be aligned to the magnetic field direction ($\vec{H}$), leading to an absence of the magnetic anisotropy. Adding the two local weak uniaxial anisotropies, $\vec{M}_1$ should rotate slightly away from the field direction towards its [10] easy axis ($\varphi_1 < \theta$) while $\vec{M}_2$ should rotate slightly away from the field direction towards its [01] easy axis ($\varphi_2 > \theta$), leading to the opposite twisting angles of $\vec{M}_1$ and $\vec{M}_2$. With the averaged magnetization angle of $\varphi_M \equiv (\varphi_2 + \varphi_1)/2$ and the small twisting angle amplitude of $\delta \equiv (\varphi_2 - \varphi_1)/2$, it is easy to show that the magnetic energy is

$$\begin{aligned} E = & -K\cos^2\varphi_1 - HM_S\cos(\theta-\varphi_1) \\ & + K\cos^2\varphi_2 - HM_S\cos(\theta-\varphi_2) \\ & = 2\cos\delta[-K\sin(2\varphi_M)\sin\delta - HM_S\cos(\theta-\varphi_M)] \end{aligned} \quad (6)$$

Minimizing the energy with respect to small δ and φ_M, we obtained the following result.

$$\delta = \frac{K}{HM_S}\sin(2\varphi_M) \quad (7)$$

$$H\sin(\theta-\varphi_M) = -\frac{K^2}{HM_S^2}\sin(4\varphi_M) \quad (8)$$

Eq. (8) corresponds to the torque Eq. (2) with a 4-fold anisotropy only ($H_{K_4} = -\frac{4K^2}{HM_S}$). Therefore, our simplified model not only reproduces correctly the 4-fold anisotropy with [11] easy magnetization axis ($H_{K_4} < 0$) but also a monotonically decrease of the anisotropy with increasing the magnetic field. In fact, the $H_{K_4} \propto 1/H$ relation in Eq. (8) describes the experimental result fairly well (dashed line in Fig. 4). The [11] easy magnetization axis can be understood easily from this oversimplified model that for magnetic field applied in the [11] direction ($\vec{H}//[11]$), it is obvious that $\vec{M}_1$ and $\vec{M}_2$ should deviate away from $\vec{H}$ direction symmetrically towards [10] and [01], respectively, leading to an averaged magnetization $(\vec{M}_1 + \vec{M}_2)/2$ exactly in the $\vec{H}$ direction (e.g. easy magnetization axis).

Last, we would like to discuss the artifact of the uniaxial magnetic anisotropy in ROTMOKE measurement. Precisely speaking, ROTMOKE measures the averaged projection of the magnetization to the [10] axis ($\cos\overline{\varphi} = \frac{1}{N}\sum_{i=1}^{N}\cos\varphi_i$) and then converts the result to the averaged magnetization angle by $\overline{\varphi} = \arccos\left(\frac{1}{N}\sum_{i=1}^{N}\cos\varphi_i\right)$. For uniform magnetization, this process makes no difference between $\overline{\varphi}$ and the magnetization angle of φ_M. Fore non-uniform magnetization, however, the magnetization angle determined by ROTMOKE is slightly greater than the averaged magnetization angle ($\overline{\varphi} > \varphi_M = \frac{1}{N}\sum_{i=1}^{N}\varphi_i$). It is this difference between $\overline{\varphi}$ and φ_M that results in the artifact of the uniaxial anisotropy in ROTMOKE because $H\sin(\theta-\overline{\varphi}) \neq H\sin(\theta-\varphi_M)$. To understand this artifact more clearly, we again use the simplified model to discuss how the difference between $\overline{\varphi}$ and φ_M results in a uniaxial anisotropy term in Eq. (8). Using the relation of $\cos\overline{\varphi} = [\cos\varphi_1 + \cos\varphi_2]/2 = \cos\varphi_M\cos\delta$ and Eq. (7), it is easy to derive the difference between $\overline{\varphi}$ and φ_M for small δ.

$$\varphi_M = \overline{\varphi} - \left(\frac{K}{HM_S}\right)^2 \sin(2\overline{\varphi})\cos^2(\overline{\varphi}) \quad (9)$$

Substitute Eq. (9) into Eq. (8) leads to

$$H\sin(\theta-\overline{\varphi}) = -\frac{K^2}{2HM_S^2}\sin(2\overline{\varphi}) - \frac{5K^2}{4HM_S^2}\sin(4\overline{\varphi}) \quad (10)$$

The first term at the right side of Eq. (10) corresponds to the uniaxial anisotropy in Eq. (2) with $H_{K_2} < 0$ and $\varphi_0 = 0$, in agreement with experimental observation. While Eq. (10) describes the experimental result qualitatively well, we would like to emphasize that the simplified model ignores many factors such as the coupling between $\vec{M}_1$ and $\vec{M}_2$ and the spatial variation within $\vec{M}_1$ and $\vec{M}_2$. All these factors are expected to modify the strength of H_{K_2} and H_{K_4} in Eq. (2) from the model. Nevertheless, our simplified model correctly reveals the physical origin of the field-dependent 4-fold anisotropy and the artifact of the uniaxial anisotropy.

4. Summary

In summary, we investigated the magnetic anisotropy of Py antidot square lattice using ROTMOKE. We showed that there exists a field-dependent magnetic anisotropy which is originated from the periodic wiggling of the magnetization in space. This inhomogeneity of the magnetic texture was confirmed by magnetic imaging using MTXM as a function of magnetic field. We also clarified the puzzle of the unexpected uniaxial magnetic anisotropy in ROTMOKE as an artifact due to the magnetization wiggling in space. Micromagnetic simulation result agrees very well with the experimental observation. We further proposed a simplified model to qualitatively explain the physical origin of the field-dependent 4-fold anisotropy and the artifact of the uniaxial anisotropy. Our investigation provides direct observation and explanation of the magnetic anisotropies in antidot square lattice.

Declaration of Competing Interest

The authors declare that they have no known competing financial interests or personal relationships that could have appeared to influence the work reported in this paper.

Acknowledgements

This work is supported primarily by US Department of Energy, Office of Science, Office of Basic Energy Sciences, Materials Sciences and Engineering Division under Contract No. DE-AC02-05CH11231 (van der Waals heterostructures program, KCWF16) which provided for T.Y.W., A.Z. and Z.Q.Q. Additional support was provided by Users with Excellence Program of Hefei Science Center CAS (No. 2021HSC-UE003) which provided for Q.L.; King Abdullah University of Science and Technology (KAUST), Office of Sponsored Research (OSR) and under the Award No. OSR-2019-CRG8-4081 which provided for X.Z.; Lawrence Berkeley National Laboratory through the Laboratory Directed Research and Development (LDRD) Program which provided for H.-S.H. and M.Y. I.; Future Materials Discovery Program through the National Research Foundation of Korea (No. 2015M3D1A1070467) and Science Research Center Program through the National Research Foundation of Korea (No. 2015R1A5A1009962) which provided for C.H. and Z.Q.Q. The operations of the Advanced Light Source at Lawrence Berkeley National Laboratory are supported by the Director, Office of Science, Office of Basic Energy Sciences, and U.S. Department of Energy under Contract No. DE-AC02–05CH11231; C.S. gratefully acknowledges support from a Kavli Energy NanoScience Institute/Heising–Simons Fellowship.

References

[1] S.D. Bader, S.S.P. Parkin, Annu. Rev. Condens. Matter Phys. 1 (2010) 71.
[2] G. Binasch, P. Grunberg, F. Saurenbach, W. Zinn, Phys. Rev. B 39 (1989) 4828.
[3] M.N. Baibich, J.M. Broto, A. Fert, F. Nguyen Van Dau, F. Petroff, P. Etienne, G. Creuzet, A. Friederich, J. Chazelas, Phys. Rev. Lett. 61 (1988) 2472.
[4] T. Miyazaki, N. Tezuka, J. Magn. Magn. Mater. 139 (1995) L231.
[5] J.S. Moodera, L.R. Kinder, T.M. Wong, R. Meservey, Phys. Rev. Lett. 74 (1995) 3273.
[6] S.H. Skjærvø, C.H. Marrows, R.L. Stamps, L.J. Heyderman, Nature Reviews Physics 2 (2020) 13.
[7] T. Shinjo, T. Okuno, R. Hassdorf, K. Shigeto, T. Ono, Science 289 (2000) 930.
[8] J. Li, A. Tan, K.W. Moon, A. Doran, M.A. Marcus, A.T. Young, E. Arenholz, S. Ma, R. F. Yang, C. Hwang, Z.Q. Qiu, Nat. Commun. 5 (2014) 4704.
[9] S. Saha, M. Zelent, S. Finizio, M. Mruczkiewicz, S. Tacchi, A.K. Suszka, S. Wintz, N. S. Bingham, J. Raabe, M. Krawczyk, L.J. Heyderman, *Phys. Rev. B* 100 (2019), 144435.
[10] J.I. Martín, J. Nogués, Kai. Liu, J.L. Vicent, Ivan K. Schuller, J. Magn. Magn. Mater. 256 (2003) 449.
[11] A. Lisfi, C.M. Williams, L.T. Nguyen, J.C. Lodder, A. Coleman, H. Corcoran, A. Johnson, P. Chang, A. Kumar, W. Morgan, Phys. Rev. B 76 (2007), 054405.
[12] L.G. Vivas, M. Vazquez, J. Escrig, S. Allende, D. Altbir, D.C. Leitao, J.P. Araujo, Phys. Rev. B 85 (2012), 035439.
[13] Sam D. Slöetjes, Einar Digernes, Christoph Klewe, Q. Padraic Shafer, M. Li, Z. Q. Yang, Alpha T. Qiu, Elke Arenholz N'Diaye, Erik Folven, Jostein K. Grepstad, Phys. Rev. B 99 (2019), 064418.
[14] U. Hartmann, Annu. Rev. Mater. Sci. 29 (1999) 53.
[15] X.M. Cheng, D.J. Keavney, Rep. Prog. Phys. 75 (2012), 026501.
[16] S.Y. Chou, Proc. IEEE 85 (1997) 652.
[17] M. Salaheldeen, L. Martínez-Goyeneche, P. Álvarez-Alonso, A. Fernández, Nanotechnology 31 (2020), 485708.
[18] Shanshan Guo, Xu. Feng, Baomin Wang, Ning Wang, Huali Yang, Pravarthana Dhanapal, Fei Xue, Junling Wang, Run-Wei Li, Adv. Mater. Interfaces 5 (2018) 1800997.
[19] Jiyun Kim, Su Eun Chung, Sung-Eun Choi, Howon Lee, Junhoi Kim, Sunghoon Kwon, Nat. Mater. 10 (2011) 747.
[20] A.O. Adeyeye, N. Singh, J. Phys. D: Appl. Phys. 41 (2008), 153001.
[21] S. Finizio, M. Foerster, M. Buzzi, B. Krüger, M. Jourdan, C.A.F. Vaz, J. Hockel, T. Miyawaki, A. Tkach, S. Valencia, F. Kronast, G.P. Carman, F. Nolting, M. Kläui, Phys. Rev. Applied 1 (2014), 021001.
[22] Na Zhu, Houchen Chang, Andrew Franson, Tao Liu, Xufeng Zhang, E. Johnston-Halperin, Mingzhong Wu, Hong X. Tang, Appl. Phys. Lett. 110 (2017), 252401.
[23] C.T. Yu, H. Jiang, L. Shen, P.J. Flanders, G.J. Mankey, J. Appl. Phys. 87 (2000) 6322.
[24] P. Vavassori, G. Gubbiotti, G. Zangari, C.T. Yu, H. Yin, H. Jiang, G.J. Mankey, J. of Appl. Phys. 91 (2002) 7992.
[25] G.N. Kakazei, X.M. Liu, J. Ding, V.O. Golub, O.Y. Salyuk, R.V. Verba, S.A. Bunyaev, A.O. Adeyeye, Appl. Phys. Lett. 107 (2015), 232402.
[26] Andreas Kaidatzis, Rafael P. del Real, Raquel Alvaro, Juan Luis Palma, José Anguita, Dimitrios Niarchos, Manuel Vázquez, Juan Escrig, José Miguel García-Martín, J. Phys. D: Appl. Phys. 49 (2016), 175004.
[27] C.C. Wang, A.O. Adeyeye, N. Singh, Nanotechnology 17 (2006) 1629.
[28] O.N. Martyanov, V.F. Yudanov, R.N. Lee, S.A. Nepijko, H.J. Elmers, R. Hertel, C. M. Schneider, G. Schönhense, Phys. Rev. B 75 (2007), 174429.
[29] Agne Ciuciulkaite, Erik Östman, Rimantas Brucas, Ankit Kumar, Marc A. Verschuuren, Peter Svedlindh, Björgvin Hjörvarsson, Vassilios Kapaklis, Phys. Rev. B 99 (2019), 184415.
[30] Xiaolong Fan, Hengan Zhou, Jinwei Rao, Xiaobing Zhao, Jing Zhao, Fengzhen Zhang, Desheng Xue, Sci. Rep. 5 (2015) 16139.
[31] J. Li, E. Jin, H. Son, A. Tan, W.N. Cao, Chanyong Hwang, Z.Q. Qiu, Rev. Sci. Instrum. 83 (2012), 033906.
[32] Peter Fischer, Dong-Hyun Kim, J. Weilun Chao, Alexander Liddle, Erik H. Anderson, David T. Attwood, Mater. Today 9 (2006) 26.
[33] J.H. Wolfe, R.K. Kawakami, W.L. Ling, Z.Q. Qiu, Rodrigo Arias, D.L. Mills, J. of Magn. Magn. Mat. 232 (2001) 36.